

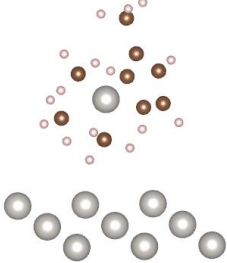
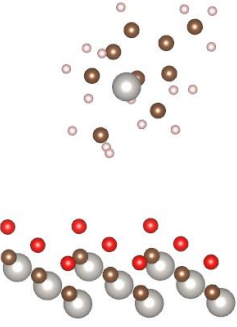
In the format provided by the authors and unedited.

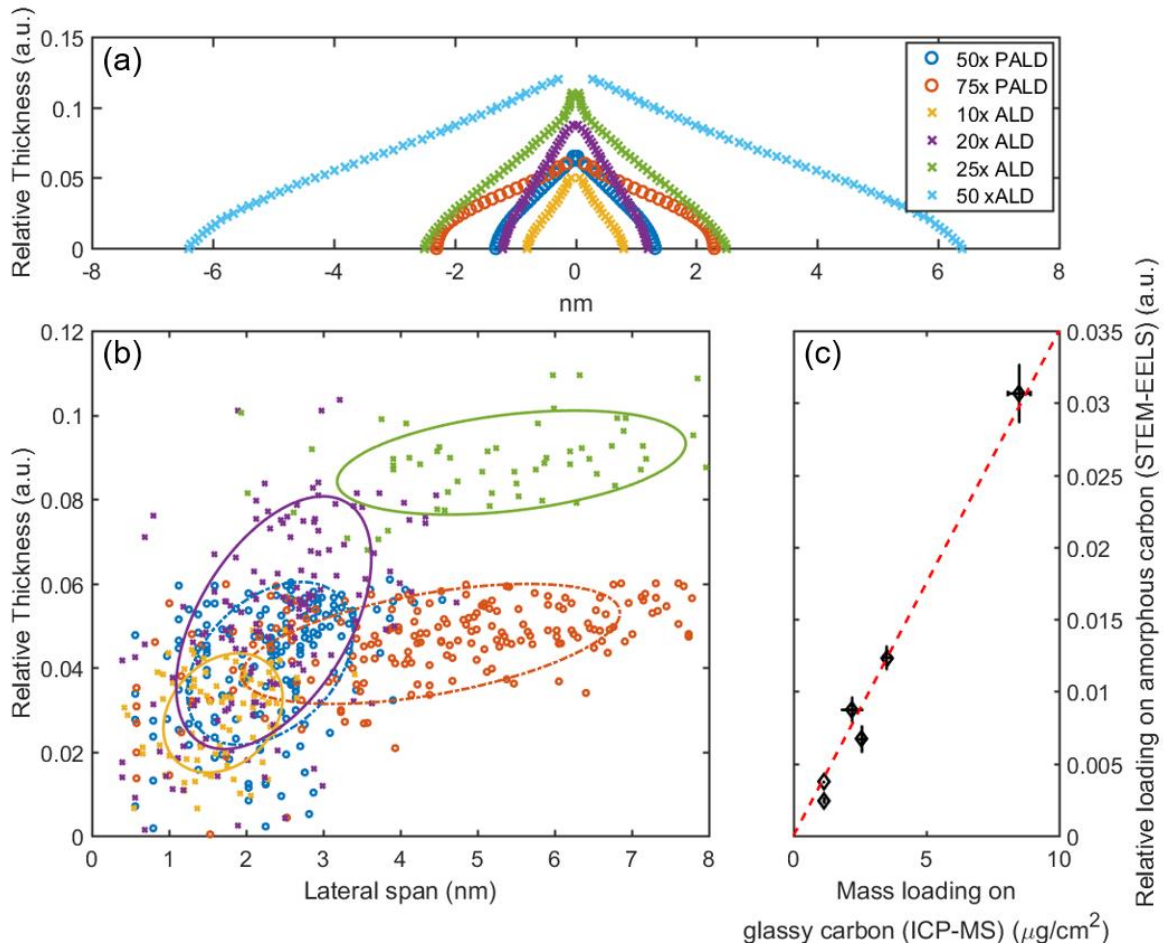
# Extending the limits of Pt/C catalysts with passivation-gas-incorporated atomic layer deposition

Shicheng **Xu**<sup>1</sup>, Yongmin **Kim**<sup>1</sup>, Joonsuk **Park**<sup>2</sup>, Drew **Higgins**<sup>3</sup>, Shih-Jia **Shen**<sup>4</sup>, Peter **Schindler**<sup>5</sup>, Dickson **Thian**<sup>6</sup>, J. **Provine**<sup>5</sup>, Jan **Torgersen**<sup>1,7</sup>, Tanja **Graf**<sup>8</sup>, Thomas D. **Schladt**<sup>8</sup>, Marat **Orazov**<sup>3</sup>, Bernard Haochih **Liu**<sup>4</sup>, Thomas F. **Jaramillo**<sup>3</sup> and Fritz B. **Prinz**<sup>1,2,7\*</sup>

<sup>1</sup>Department of Mechanical Engineering, Stanford University, Stanford, CA, USA. <sup>2</sup>Department of Material Science and Engineering, Stanford University, Stanford, CA, USA. <sup>3</sup>Department of Chemical Engineering, Stanford University, Stanford, CA, USA. <sup>4</sup>Department of Materials Science and Engineering, National Cheng Kung University, Tainan, Taiwan. <sup>5</sup>Department of Electrical Engineering, Stanford University, Stanford, CA, USA. <sup>6</sup>Department of Applied Physics, Stanford University, Stanford, CA, USA. <sup>7</sup>Department of Mechanical and Industrial Engineering, Norwegian University of Science and Technology, Trondheim, Norway. <sup>8</sup>Volkswagen Group Research, Wolfsburg, Germany. \*e-mail: [fprinz@stanford.edu](mailto:fprinz@stanford.edu)

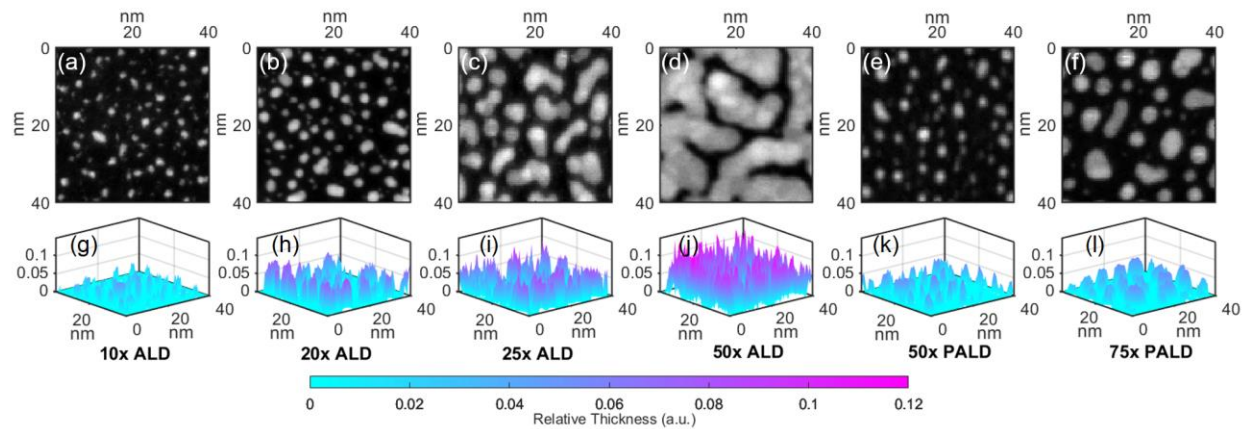
Supplementary Table 1. Adsorption energy of physisorption and chemisorption of the Pt precursor, MeCpPtMe<sub>3</sub> onto Pt (111) and CO passivated Pt (111). Pt atoms are in silver, carbon atoms are in brown, hydrogen atoms are in linen, and oxygen atoms are in red.

Structure	Adsorption Energy (eV)
	-0.37
	-0.059

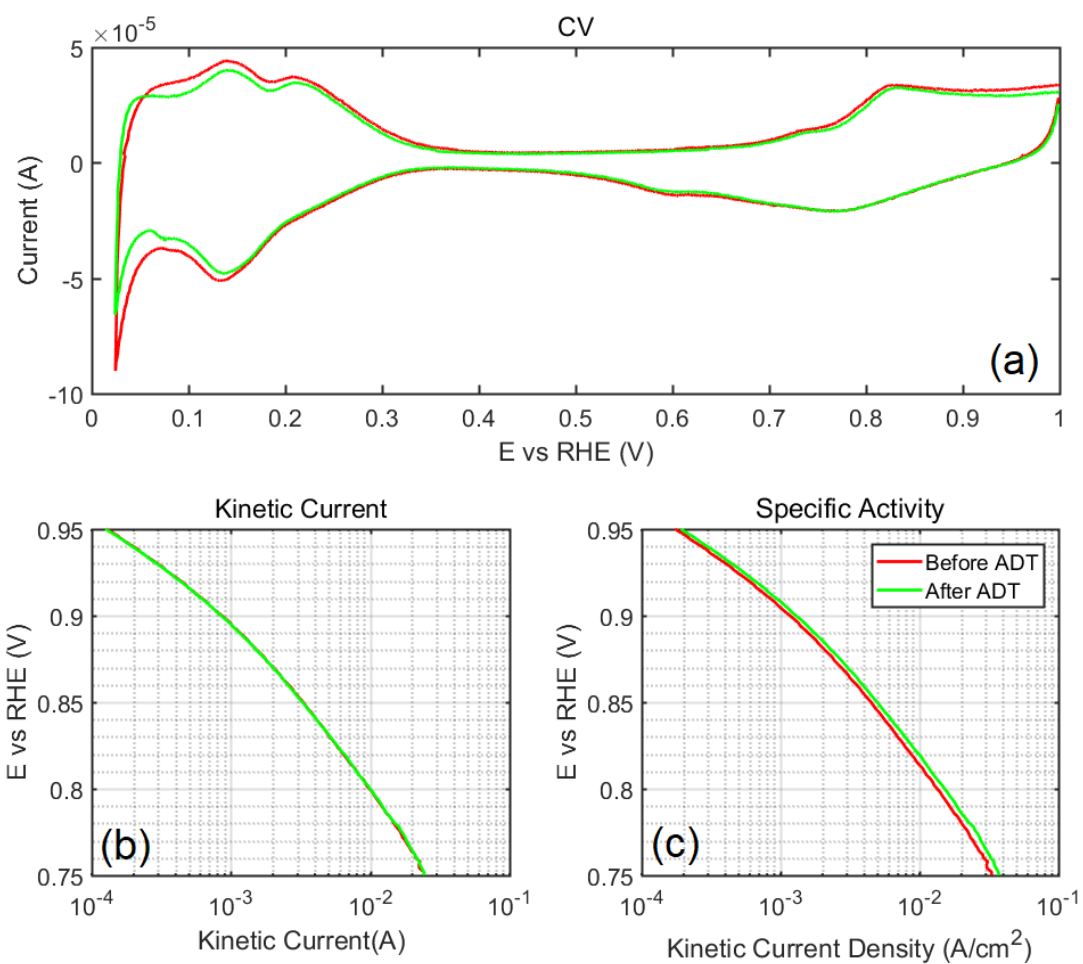


Supplementary Figure 1. (a) Average cross-sectional profile of the particles by 10x, 20x, 25x, 50x ALD and 25x, and 50x PALD as deduced from thickness statistics. These average profiles in a cylindrical coordinate from top down are calculated with the Supplementary Equation 1, where  $\varphi_h$  and  $r_h$  are the relative proportion of pixels and the radii of the projected particle cross section, respectively, with height around relative thickness of  $h$ .  $h_{top}$  is the largest relative thickness value associated with a certain sample, and  $A$  is a normalizing factor. (b) Lateral width versus height of each particle made by the above mentioned ALD/PALD processes with 60 % confidence ellipses to correlate horizontal and vertical dimensions, as a statistical view of particle geometries complementing the average particle profiles shown in (a). For the normal ALD, particles grow in both width and height as a function of cycle number, especially below 25 cycles. A clear transition from the 20 to 25 cycles shown in (b) indicates a change in growth mode from island growth to island coalescence. The same transition is found in the PALD cycles but occurred between 50-75 cycles and converged to a lower thickness. (c) Relative thickness mapping by STEM-EELS compared with mass loading determined by ICP-MS. The average values and error bars were obtained as the standard deviation of at least three independent repetitions of the measurements.

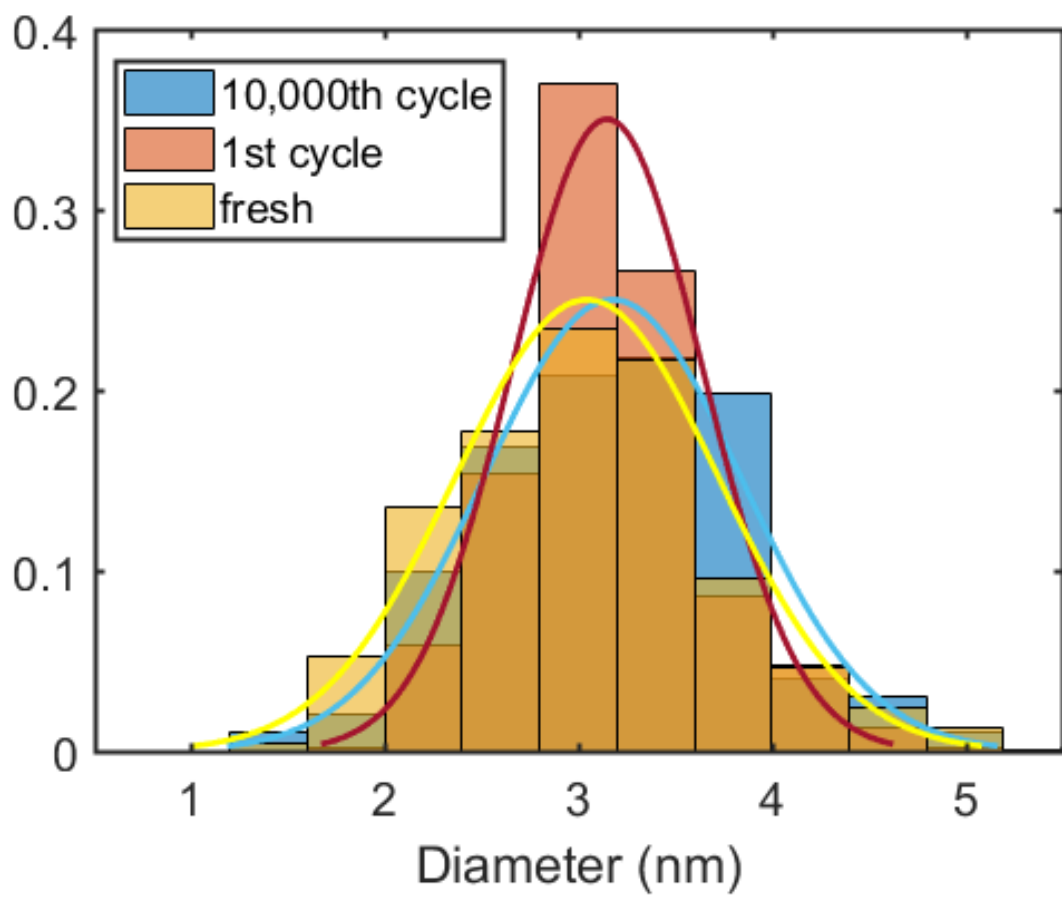
$$r_h^2 - r_{h_{top}}^2 = A \sum_{h_{top}}^h \varphi_h \quad (1)$$



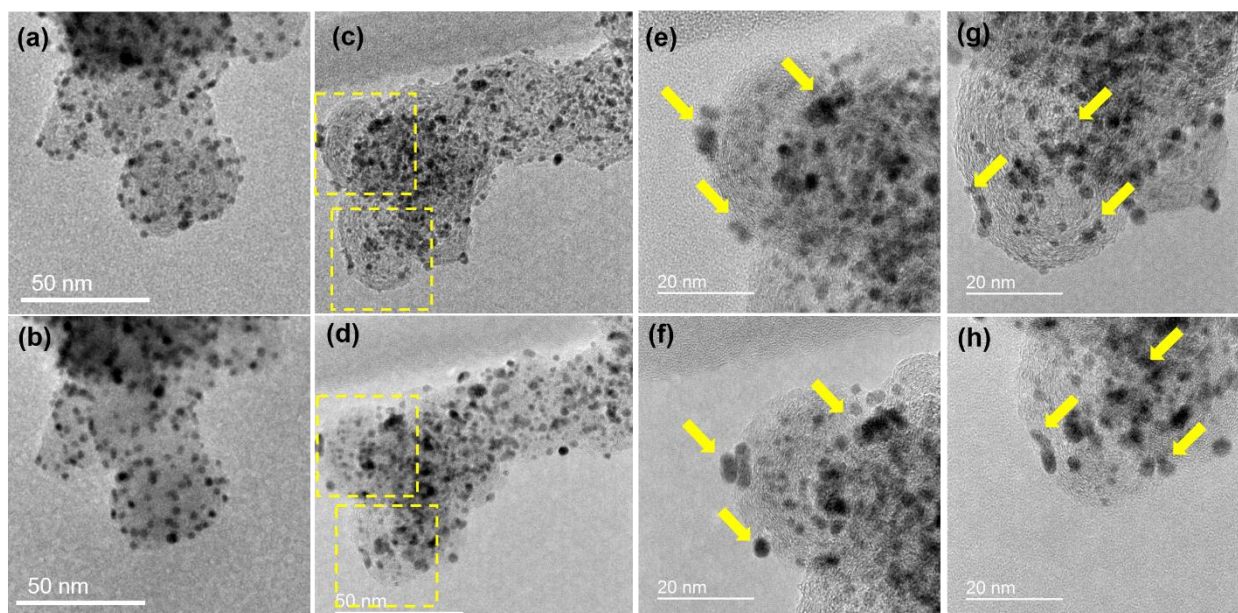
Supplementary Figure 2. STEM-EELS annular dark-field micrographs (a-f) and 3D views of relative thickness mappings (g-l) on (a-d, and g-j) 10, 20, 25 and 50 cycles of ALD and (e-f, and k-l) 50 and 75 cycles of PALD deposited on carbon thin films to complement Figure 1.



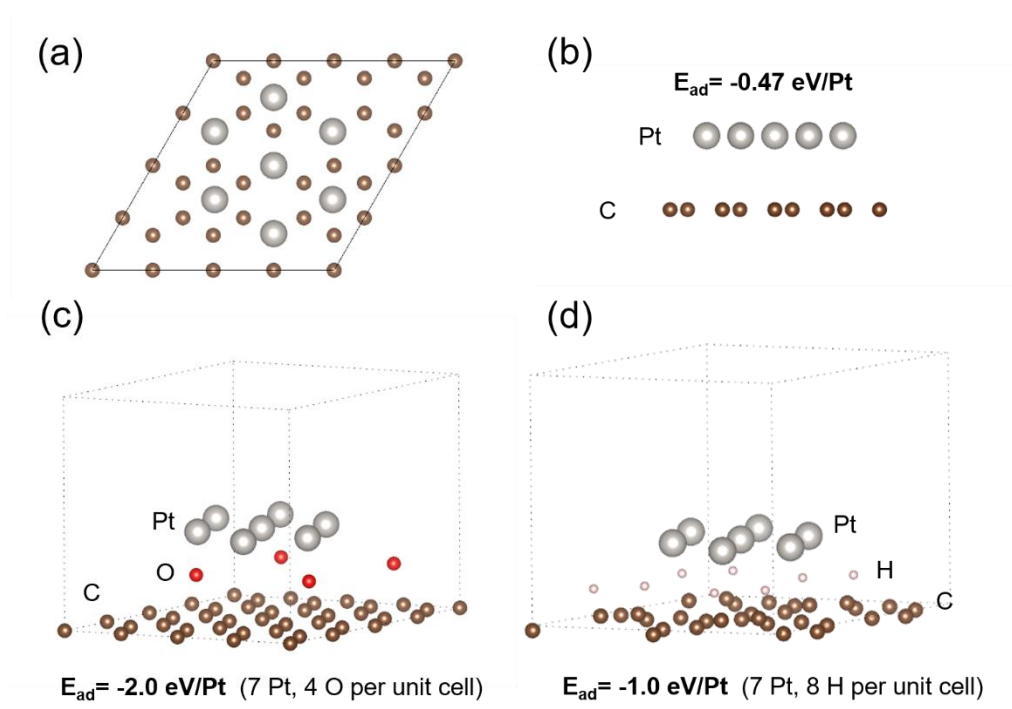
Supplementary Figure 3. Cyclic Voltammetry curves (a) of 40x PALD Pt/C samples before and after 10,000 ADT in  $O_2$ , with projected kinetic current density (b) and specific activity (c) compared.



Supplementary Figure 4. Pt particle equivalent diameter statistics of Pt<sub>PALD</sub> 40x/C catalysts before and after oxygen reduction reaction tests.

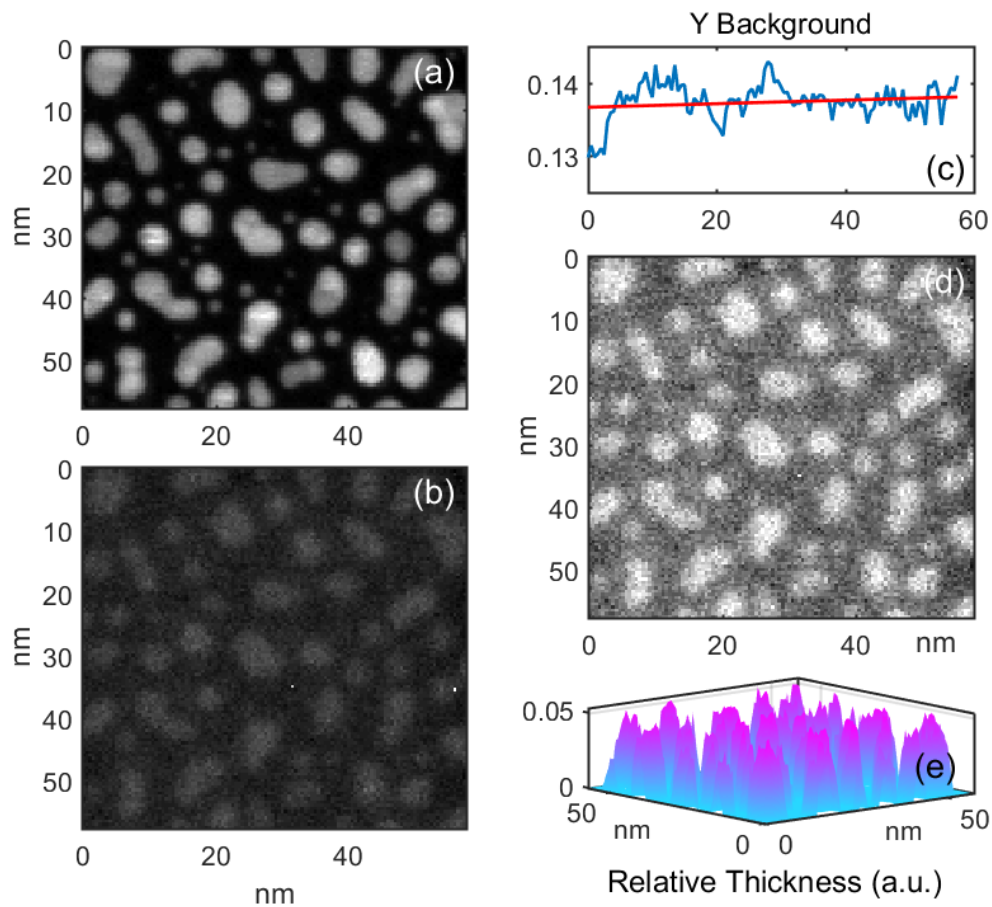


Supplementary Figure 5. TEM images of (a, b) Pt<sub>PALD</sub> 40x/C and (c, d) Pt/HSC before (a, c) and after (b, d) electron beam irradiation (200 kV). With respect to a noticeable change on Pt/HSC from (c) and (d), local change of Pt morphologies before (e, g) and after (f, h) electron beam irradiation is highlighted in the boxes and contrasted with higher magnification. The yellow arrows indicate spots where particle coalescence occurred. Electron beam irradiation<sup>1</sup> was applied to Pt<sub>PALD</sub> 40x/C and Pt/HSC catalysts, with a beam dose of 1400 electron/Å<sup>2</sup>/s. After 5-minute electron beam irradiation on both samples, a similar trend from Figure 4 was observed as Pt<sub>PALD</sub> 40x/C underwent significantly fewer morphological changes compared to Pt/HSC (a/b compared to c/d). It is noted from (f) and (h) that particles that are closely spaced are subject to coalescence. Small particles also grow bigger with shrinking interparticle distances. For the Pt<sub>PALD</sub> 40x/C, there are noticeably a few cases of closely spaced particles coalesced into large ones as well. Nevertheless, given a lower portion of closely spaced particles, coalescence is not significant on Pt<sub>PALD</sub> 40x/C compared to Pt/HSC.



Supplementary Figure 6. Binding energy estimate with a Pt<sub>7</sub>(111) slab on (a, b) a pristine graphene surface, (c) graphene surface with oxygen, and (d) graphene surface with sp<sup>3</sup> carbon.





Supplementary Figure 7. A procedure to obtain background corrected STEM-EELS-based relative thickness map with the example of 75x PALD sample. (a) ADF image, (b) uncorrected STEM-EELS-based thickness map, (c) calculated background profile in the y direction, (d) background corrected relative thickness map, and (e) a three-dimensional view of (d). Considering that carbon contamination was built up in the direction of the scans, background subtraction (c) was performed along the y direction. Median values of the background pixels were collected in each line and plotted. A linear fit was applied and the results were used as the relative thickness of the carbon substrate. By subtracting this background signal from (b), one can obtain the Pt particle thickness map as shown in (d). The 3D profile as shown (e) was filtered by applying a two-dimensional Gaussian smoothing kernel with standard deviation of 0.5 to suppress noise.

Supplementary Table 2. The evaluated tip radius of curvature as the function of distance to tip end (Z-range) for Tip 1 and Tip 2 in this study for tip deconvolution<sup>2,3</sup> of their physical profiles.

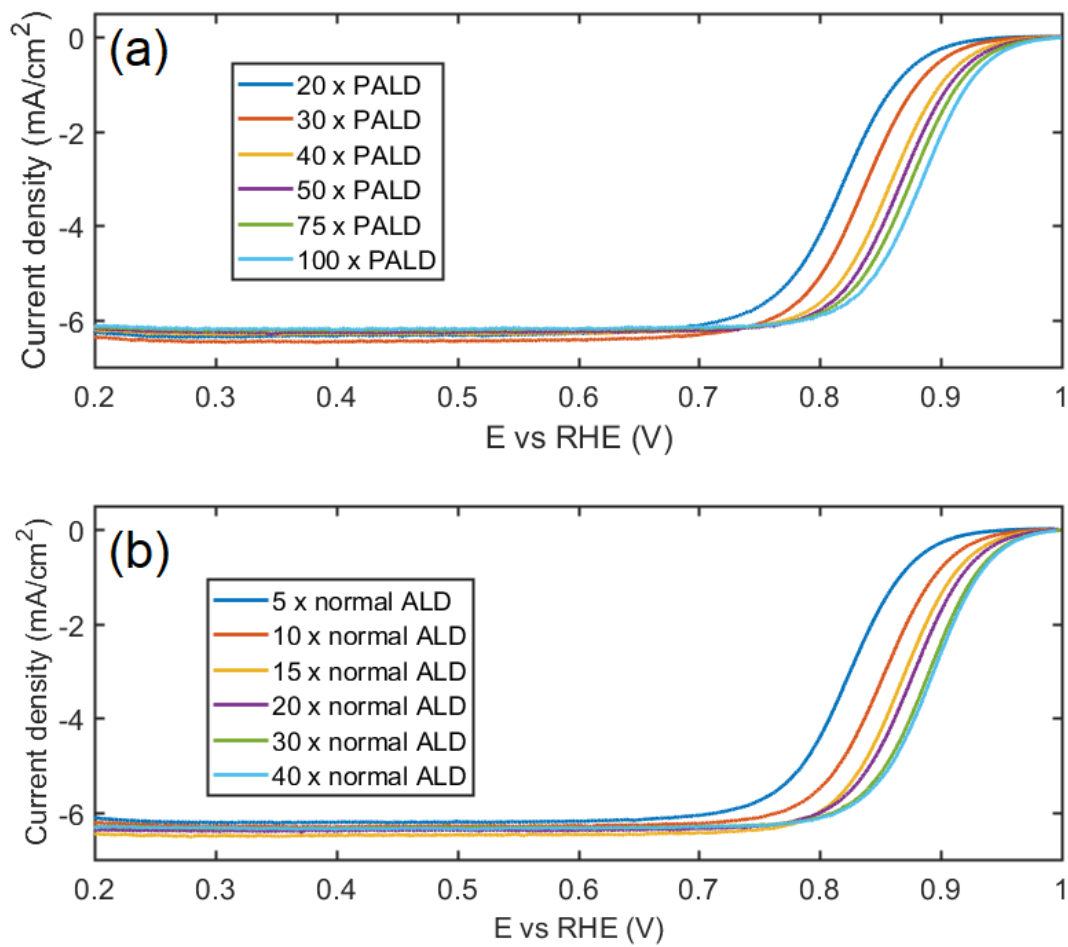
Z range/ nm	Tip 1/ nm	Tip 2/ nm
0~1	1.53	1.81
0~2	3.23	3.47
0~3	4.52	5.63
0~5	6.49	8.57
0~10	8.71	11.74

Supplementary Table 3. Nanoparticle analysis for 50x PALD sample with raw AFM, tip deconvolution 1, and tip deconvolution 2 morphology. The average width and height values are sampled with 11 randomly selected nanoparticles. The 50x PALD nanoparticles are circular.

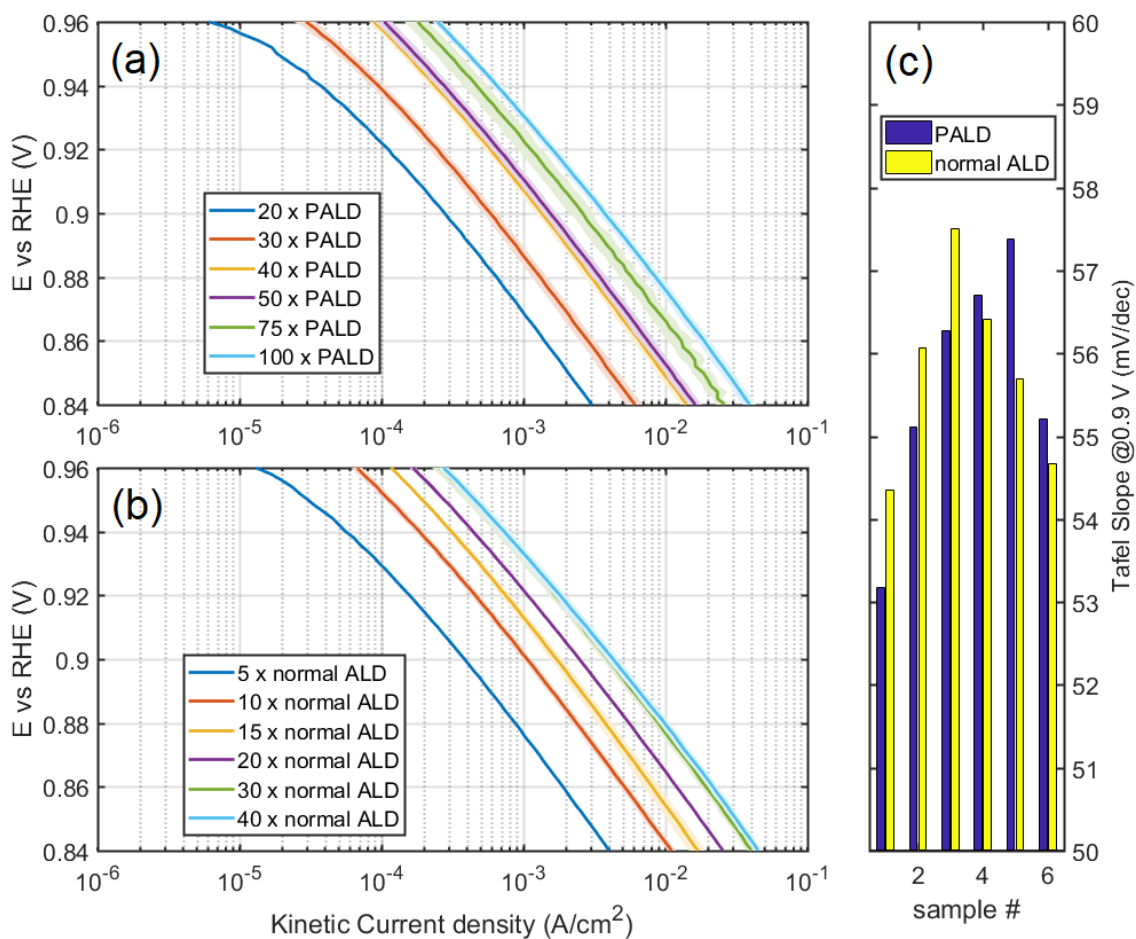
Sample	NP width (average)/ nm	NP height (average)/ nm	Roughness (Ra)/ nm	Roughness (Rq)/ nm
Raw	7.26	1.32	0.231	0.316
Tip decon 1	6.45	1.22	0.213	0.288
Tip decon 2	7.12	1.25	0.226	0.305

Supplementary Table 4. Nanoparticle analysis for 20x ALD sample with raw AFM, tip deconvolution 1, and tip deconvolution 2 morphology. The 20x ALD nanoparticles have elongated oval shapes, and thus both long and short axes cross-sectional data are listed.

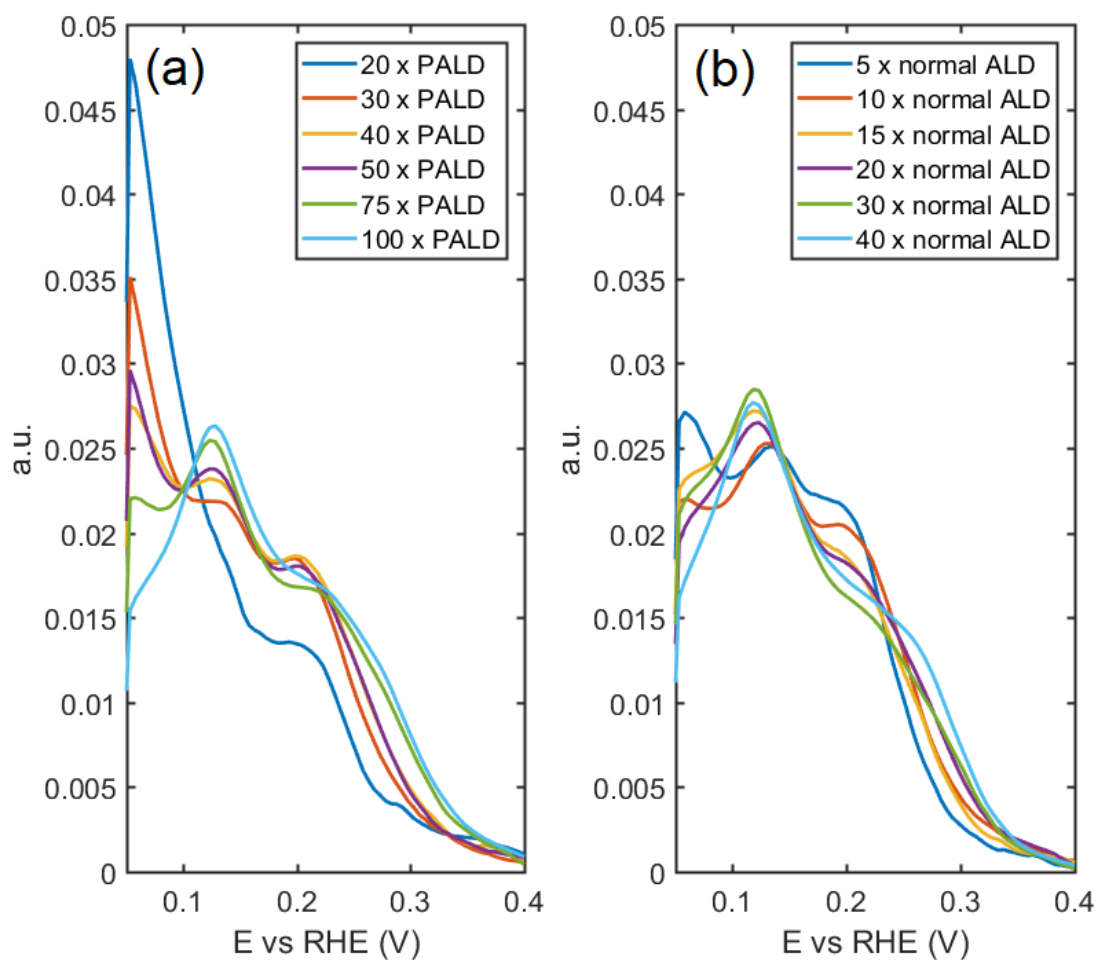
Sample	Long axis (average)/ nm	Long axis Height (average) /nm	Short axis (average)/ nm	Short axis Height (average) /nm	Roughness (Ra) /nm	Roughness (Rq) /nm
Raw	12.06	2.02	9.33	1.64	0.472	0.622
Tip decon 1	11.38	1.78	8.51	1.60	0.436	0.583
Tip decon 2	11.66	1.93	8.92	1.64	0.453	0.594



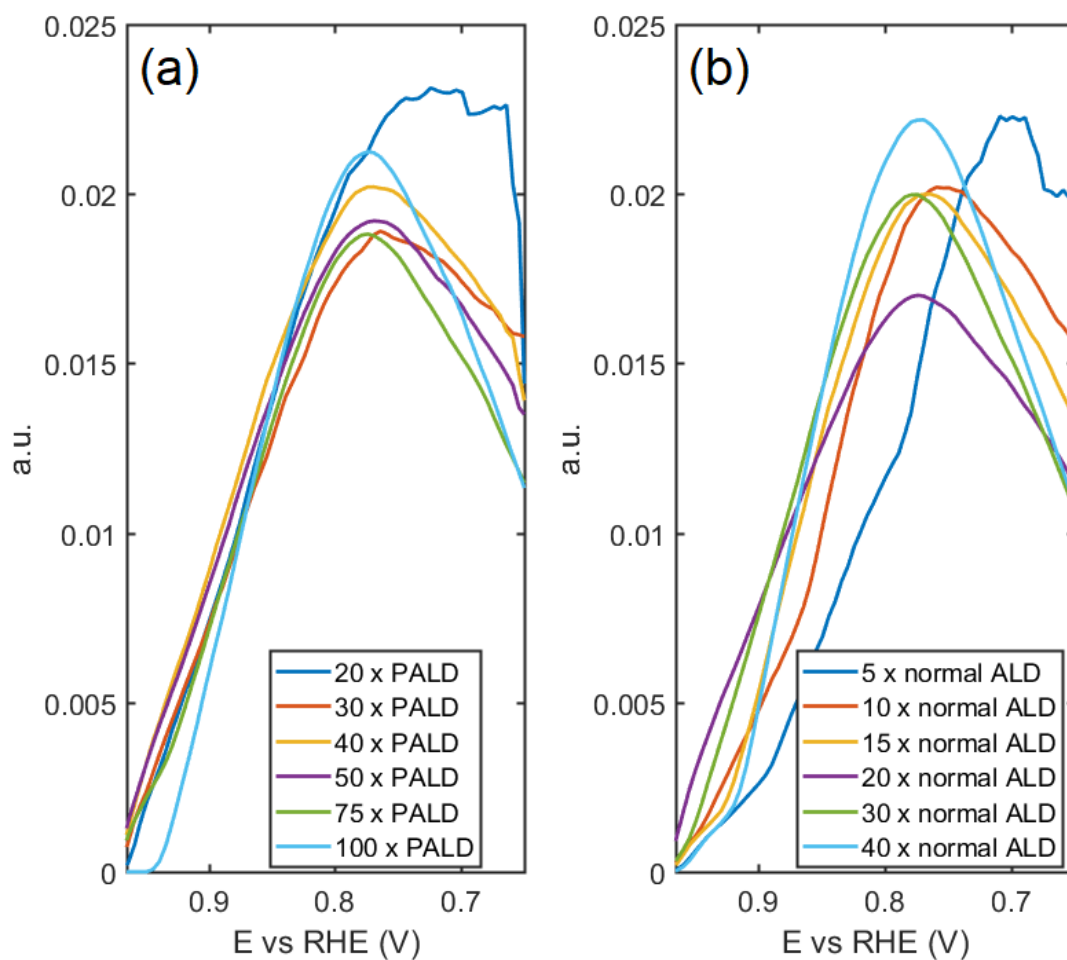
Supplementary Figure 8. ORR linear sweep voltammetry of Pt deposited on glassy carbon electrode by (a) PALD and (b) ALD.



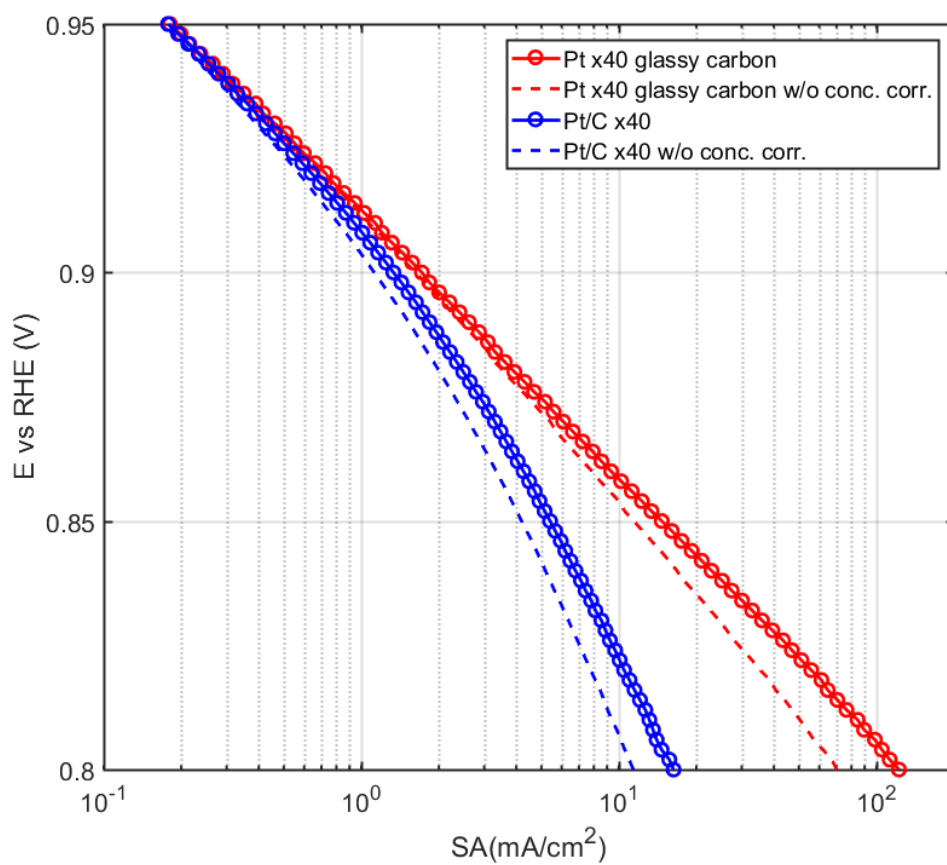
Supplementary Figure 9. Tafel plots of Pt deposited on glassy carbon electrodes by (a) PALD and (b) ALD and (c) extracted Tafel slopes at 0.9 V vs RHE. The transparent bands indicate the standard deviation of measurements from five replicate samples.



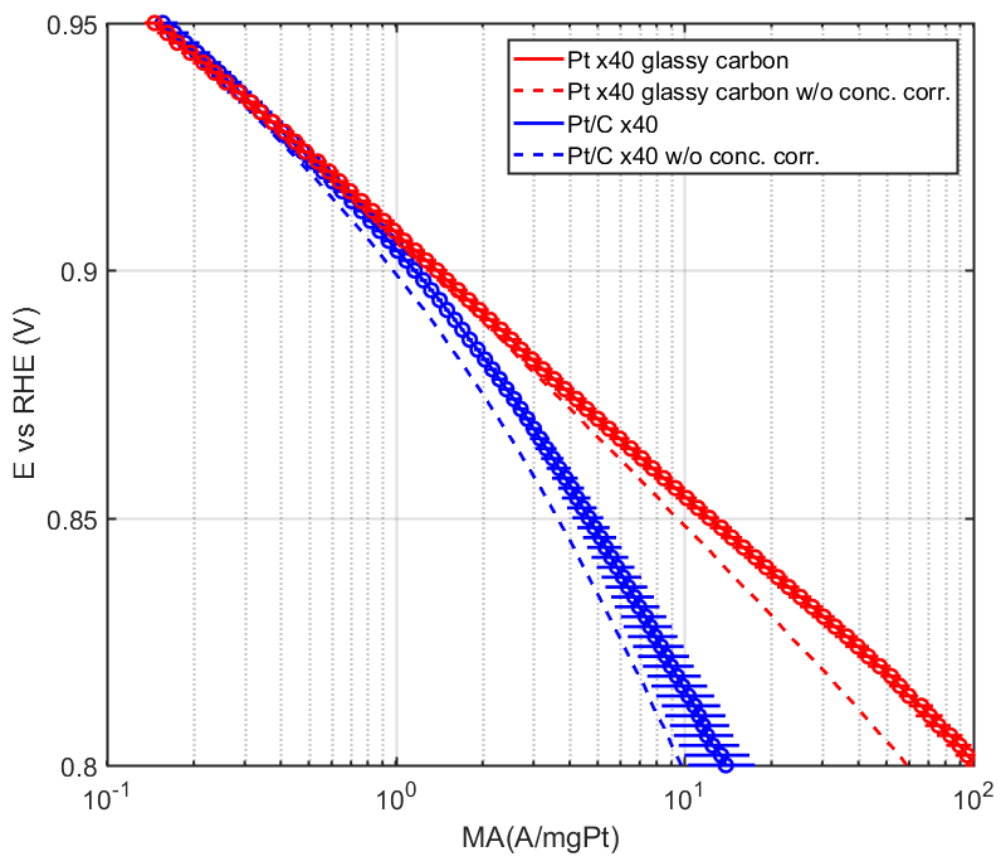
Supplementary Figure 10. Hydrogen under potential deposition (HUPD) part of the Cyclic Voltammetry curves (normalized by electrochemical active areas) of Pt deposited on glassy carbon electrodes by (a) PALD and (b) ALD. The peaks at around 0.05 V associated with lower PALD cycles are attributed to exposed glassy carbon surfaces that are not covered by Pt.



Supplementary Figure 11. Oxygen species desorption part of the cyclic voltammetry curves (normalized by electrochemical active areas) of Pt deposited on glassy carbon electrodes by (a) PALD and (b) ALD.

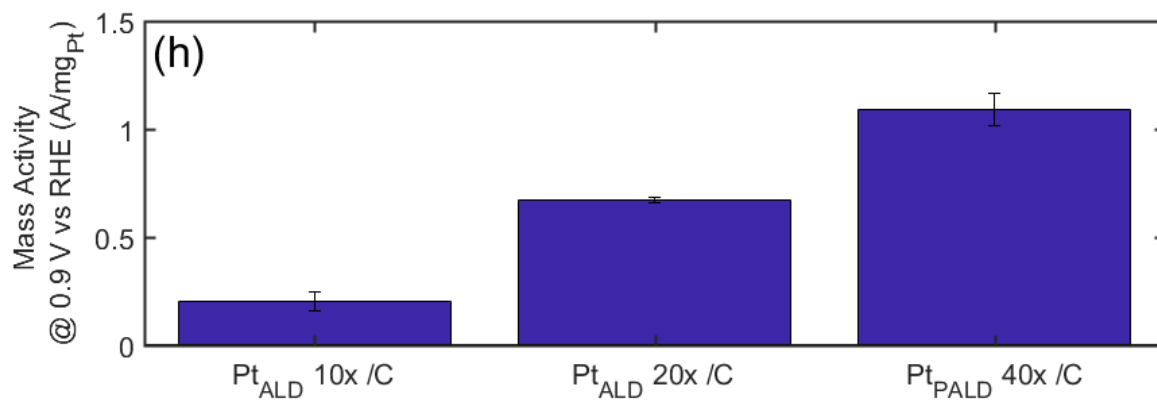
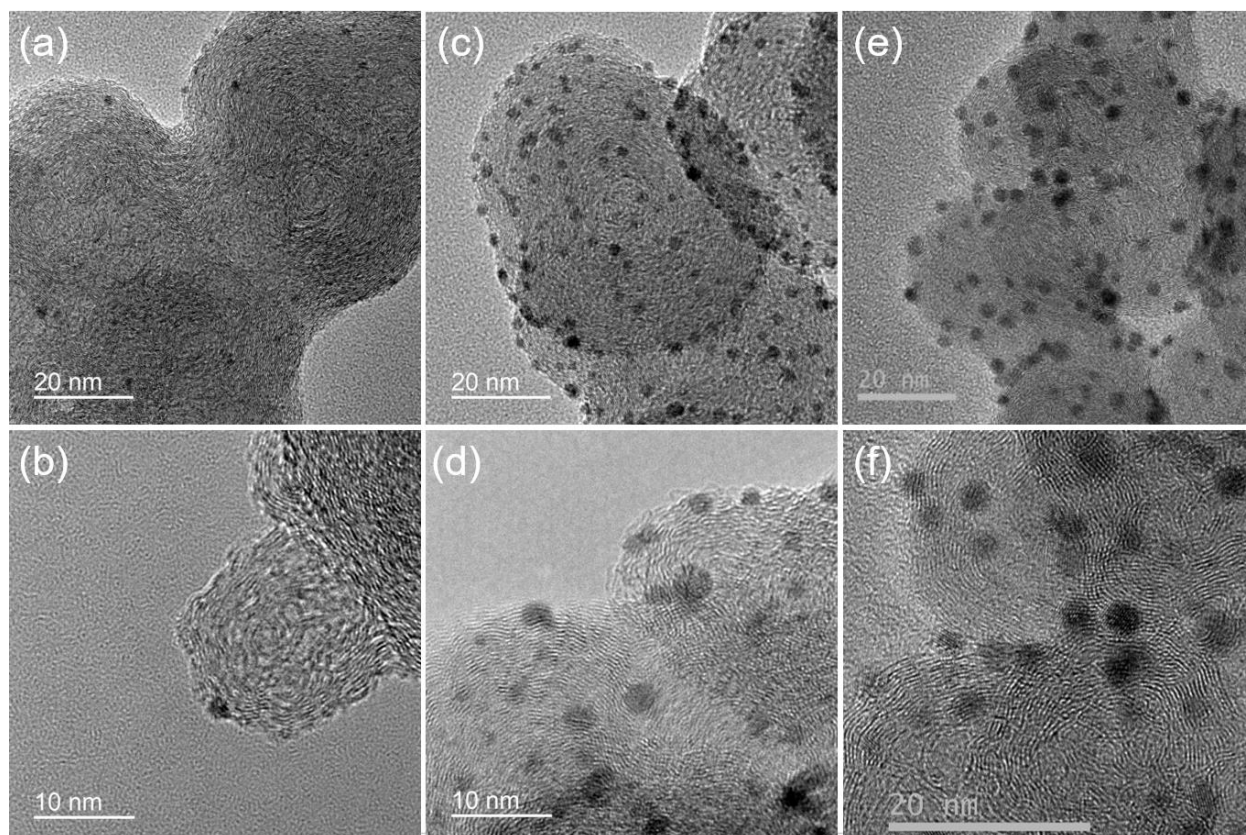


Supplementary Figure 12. Comparison of specific activities of 40x PALD of Pt on glassy carbon electrode and Pt/C catalysts. A concentration correction is applied to correct the Nernstian overpotential associated with high catalyst loading.



Supplementary Figure 13. Comparison of mass activities of 40x PALD for Pt on glassy carbon electrode and Pt/C catalysts. The error bars indicate the standard deviation of measurements from three replicate samples.





Supplementary Figure 14. TEM images of (a, b) 10x ALD, (c, d) 20x ALD, and (e, f) 40x PALD on the same carbon powder. The mass activities (h) of these catalysts evaluated using the same solvent/water ratio and ionomer/carbon ratio as the Pt<sub>PALD</sub> 40x/C samples as described in the methods section are compared with a bar plot. The error bars indicate the standard deviation of measurements from three replicate samples.

## Supplementary References

1. Cichocka, M. O. *et al.* In situ observations of Pt nanoparticles coalescing inside carbon nanotubes. *RSC Adv.* **4**, 49442–49445 (2014).
2. Liu, H.-C., Dahlen, G. A. & Osborne, J. R. in *Applied Scanning Probe Methods VIII* 31–75 (Springer Berlin Heidelberg, 2008). doi:10.1007/978-3-540-74080-3\_2
3. Dahlen, G. A. *et al.* Critical dimension AFM tip characterization and image reconstruction applied to the 45-nm node. in *SPIE Microlithography* (ed. Archie, C. N.) **6152**, 61522R (International Society for Optics and Photonics, 2006).